Mechanism of reflection high-energy electron-diffraction intensity oscillations during molecular-beam epitaxy on a Si(001) surface

K. Mitsuishi and I. Hashimoto

Department of Physics, Science University of Tokyo, 1-3 Kagurazaka, Shinjuku-ku, Tokyo 162, Japan

K. Sakamoto and T. Sakamoto

Electrotechnical Laboratory, 1-1-4 Umezono, Tsukuba 305, Japan

K. Watanabe

Tokyo Metropolitan Technical College, 1-10-40 Higashiohi, Shinagawa-ku, Tokyo 140, Japan

The mechanism for the reflection high-energy electron-diffraction intensity oscillations during molecular-beam-epitaxy growth on the Si(001) surface is examined by using multiple-scattering theory, combined with the birth-death model. The monolayer and bilayer mode oscillations that occur along the [010] and the [1$\bar{1}$0] directions can be reproduced well. It turns out that these oscillation modes are mainly caused by the interaction among the specular, two side bulk, and two surface reconstruction beams on the zeroth Laue zone, which have monolayer or bilayer mode periodicity.

I. INTRODUCTION

Recent developments in reflection high-energy electron diffraction (RHEED) have made it possible to directly observe not only fine surface diffraction patterns but also beam intensity oscillations during crystal growth. Of considerable importance to the development of molecular-beam epitaxy (MBE) has been the application of RHEED as an *in situ* surface analytical technique. For semiconductors, the technique of RHEED intensity oscillation has been used routinely to control thin film and superlattice growth during MBE growth.[1-3]

In the case of Si(001) MBE on single and double domains, it is reported that the period of the RHEED oscillation corresponds to a biatomic-layer height when the incident-beam azimuth is along the [1$\bar{1}$0] direction, and corresponds to a monatomic height when the azimuth is along the [010] direction.[4-8] However, there are no conclusive interpretations of these intensity oscillations, while several treatments using the kinematical theory and the multiple-scattering theory including the effects of surface steps or surface reconstruction have been suggested.[9-11]

The main aim of this paper is to make clear the mechanism of the RHEED monolayer and bilayer intensity oscillations on the Si(001) surface.

II. CALCULATION

In our calculation, the asymmetric dimer model[12-14] is adopted for the Si(001) surface, whereas there has been considerable controversy concerning the symmetric and asymmetric dimer models. The displacements of the surface dimer atoms are taken as the same as those of Chadi, and those of atoms under the surface dimers are ignored because these displacements are about one-seventh those

of surface dimer atoms. Using this structure model, the surface potential $V(g,z)$, where g are the two-dimensional reciprocal lattice vectors and z is the coordinate perpendicular to the surface, can be obtained for both the 2×1 and 1×2 surface structures. As shown in Fig. 1, the potential $V(g,z)$ can be divided into four layers having 5.43/4 Å thickness, like the spreading out $V^{sp}(g)$, top $V^{top}(g)$, lower $V^{lower}(g)$, and bulk $V^{bulk}(g)$ parts. The spreading out part $V^{sp}(g)$ is assumed to be a layer in a vacuum region in order to avoid artificial ceasing of potential at surface/vacuum interface. The top part potential $V^{top}(g)$ corresponds to one layer of dimer atoms. Due to the large displacements of the dimer atoms at the top layer, the lower potential $V^{lower}(g)$ deviates from the bulk one, even though the displacements of lower-layer atoms are themselves ignored. The bulk part potential $V^{bulk}(g)$ has the same periodicity as the bulk one.

During MBE growth, the system is considered to be made of 1×2 and 2×1 surface structures, and these surface structures occur alternately, as shown in Fig. 2, where odd-numbered layers correspond to the 2×1 sur-
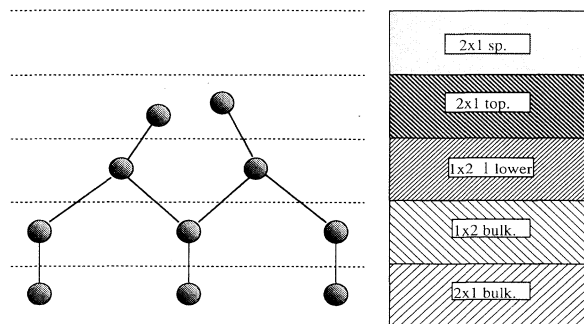
FIG. 1. The schematic diagram of corresponding atom position for 2×1.
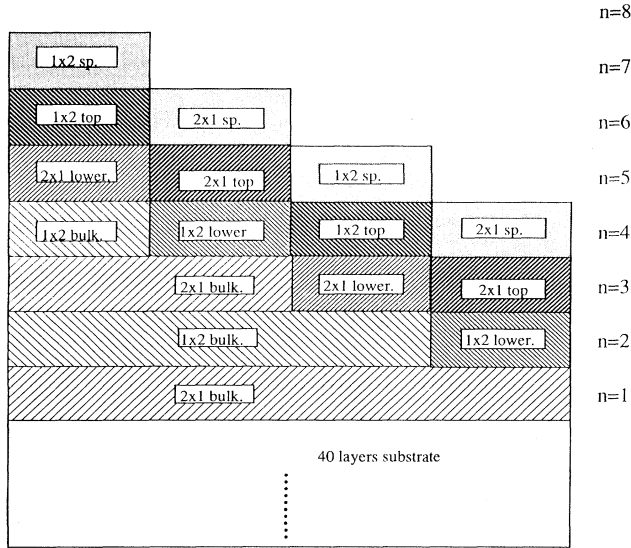
FIG. 2. The schematic diagram of potential construction for MBE growth.

face structure and even-numbered layers correspond to the 1×2 surface structure. Therefore, the potentials for the growing system are simply obtained at each layer by adding up these surface potentials in proportion to the exposed ratio determined by the coverage value θ. In dynamical calculations, the substrate potential, which consists of 40 layers, is also included.

A simple birth-death model[15] was used to obtain the coverage value θ in order to explore fundamental behavior of oscillation during growth. By using the solid-on-solid approximation[16] excluding vacancies and overhangs, the coverage θ of the nth surface layer satisfies the following set of differential equations:[15]

$$\frac{d\theta_n}{dt} = \frac{1}{\tau}(\theta_{n-1}-\theta_n)+D(\theta_{n+1}-\theta_{n+2})(\theta_{n-1}-\theta_n)$$
$$-D(\theta_n-\theta_{n+1})(\theta_{n-2}-\theta_{n-1}) ,$$

where τ is the time to deposit a monolayer and D a diffusion parameter. For all the calculations, $1/\tau=1$ and diffusion parameter $D=3500$ were chosen so as to make a nearly perfect layer-by-layer growth mode. The growth was started from the states $\theta_1=1$ and $\theta_n=0$ ($n\neq1$), which correspond to the single domain surface.

By using the coverage $\theta_n(t)$ obtained from a set of differential equations, the exposed ratio at the nth layer can be expressed as

$$C_n^s=\theta_n-\theta_{n+1} .$$

So the spreading out, top, and lower part potentials are described as

$$V_{n+1}^{sp}(g)=C_n^s V_{sp}(g) ,$$

$$V_n^{top}(g)=C_n^s V^{top}(g) ,$$

and

$$V_{n-1}^{lower}(g)=C_n^s V^{lower}(g) .$$

For the bulk part potential, a ratio is described as

$$C_n^{bulk}=\theta_{n+2} ,$$

and the bulk part potential is written as

$$V_n^{bulk}(g)=C_n^{bulk} V^{bulk}(g) .$$

Therefore, a total potential of a system is obtained by the following summation:

$$V(g)=\sum_n V_n(g) ,$$

where

$$V_n(g)=V_n^{top}(g)+V_n^{lower}(g)+V_n^{sp}(g)+V_n^{bulk}(g) .$$

III. RESULT AND DISCUSSION

For the multiple-scattering calculations, Ichimiya's method was used and each nth layer was also divided into 30 slices parallel to a surface.[17,18,11] It is known that the treatment gives rise to the same result as that obtained by Maksym and Beeby.[19,20] Inelastic scattering was included as an imaginary part of a potential taken as 10% of the real part. The accelerating voltage and incident angle were fixed at 40 kV and 14 mrad in order to create the same condition as the experiment.[5,7]

In Figs. 3 and 4, the RHEED intensity oscillations of the three different diffraction spots are plotted for the $[1\bar{1}0]$ and $[010]$ azimuths, together with beam sets for the $[1\bar{1}0]$ and $[010]$ directions and their schematic diffraction patterns. The beam numbers included in these calcula-
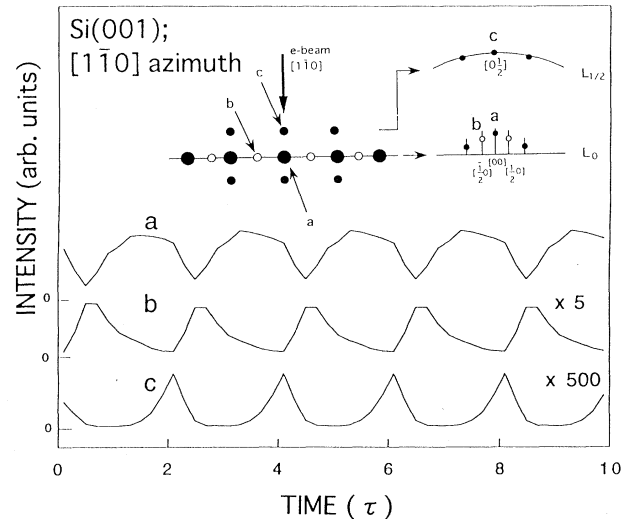
FIG. 3. The result of 15-beam calculation of RHEED intensity oscillations of the three different diffraction spots taken in the $[1\bar{1}0]$ azimuth: (a) specular beam, (b) 2×1 reconstruction spot, and (c) 1×2 reconstruction spot. Inset figures show schematically the reciprocal lattice points of $(001)2\times1+1\times2$ taken into the calculation and a corresponding diffraction pattern: (a) large solid circles, (b) small open circles, and (c) small solid circles represent the bulk diffraction, 2×1 reconstruction-related spots, and 1×2 reconstruction-related spots, respectively.
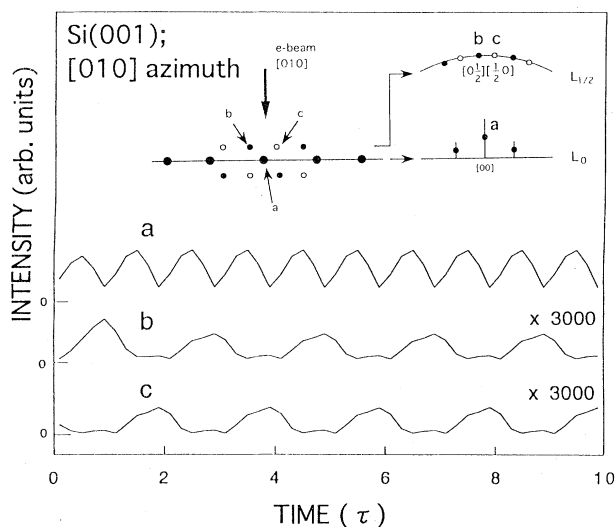
FIG. 4. The result of 13-beam calculation of RHEED intensity oscillations of the three different diffraction spots taken in the [010] azimuth: (a) specular beam, (b) 2×1 reconstruction spot, and (c) 1×2 reconstruction spot. Inset figures show schematically the reciprocal lattice points of (001)2×1+1×2 taken into the calculation and a corresponding diffraction pattern: (a) large solid circles, (b) small open circles, (c) small solid circles represent the bulk diffraction, 2×1 reconstruction-related spots, and 1×2 reconstruction-related spots, respectively.

tions are 15 and 13 beams for the [1$\bar{1}$0] and [010] azimuths, respectively. It has been confirmed that the number of beams and the number of slices are large enough for accurate calculations.

In the case of the [1$\bar{1}$0] azimuth, our method reproduces well biatomic-layer mode oscillation for 2×1 and 1×2 reconstruction beams as well as biatomic-layer mode oscillation for the specular beam. The period for the biatomic-layer mode oscillation consists of the biatomic-layer height growth. However, there is a π out of phase between the a and b beams, while $\pi/2$ (Refs. 5 and 7) or π (Ref. 8) phase differences are observed in the experiments.

As for the [010] azimuth, the present calculations are in good agreement with biatomic-layer mode oscillation for 1×2 and 2×1 reconstruction beams, and monatomic-layer mode oscillations for the specular beam. These oscillation modes correspond accurately to monolayer and bilayer height growths. In addition, these phases agree with the experiment. However, the intensities of the reconstruction beams on the half Laue zone for both [1$\bar{1}$0] and [010] azimuths are much smaller than those of the experiments. The reasons for these large differences are considered as follows. One is the simplified surface structure which is far from a realistic surface excluding irregular arrays of steps and islands. Another is that there may be a slight difference in incident-beam angle between experiment and calculation, because the discrepancy of intensity is improved to one-sixth with a slightly shallower incident angle of 12 mrad.

Now, we return to a qualitative description in order to
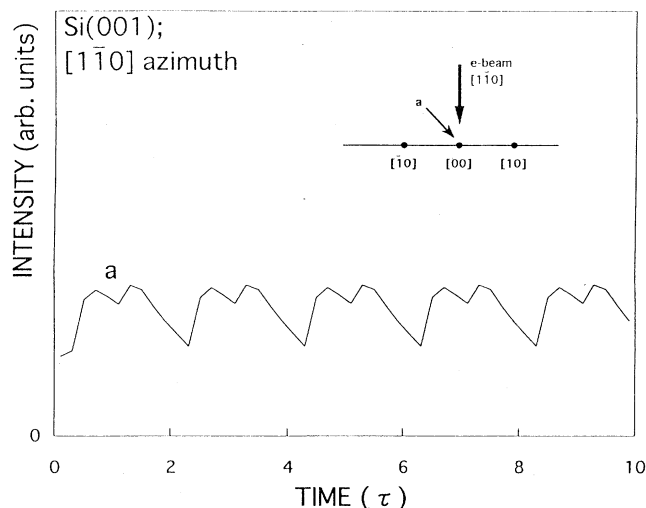
FIG. 5. The result of 3-beam calculation of RHEED intensity oscillations in the [1$\bar{1}$0] azimuth. Inset figures show the reciprocal lattice points of (001)2×1+1×2 taken into the calculation.

clarify the mechanism of oscillations. Since the RHEED intensities are controlled by a few beams on the zeroth Laue zone,[21] we have carried out the multiple-scattering calculations for [1$\bar{1}$0] and [010] azimuths in a simplified way where the surface reconstruction is not taken into account. The results in Figs. 5 and 6 are obtained in three-beam calculations; i.e., only the specular-beam and two side bulk beams are taken into account where these beams are evanescent waves.

As the [10] and [$\bar{1}$0] beams have the bilayer mode period against surface normal direction like the 1×2 and 2×1 reconstruction beams and the [$\bar{1}$1] and the [1$\bar{1}$] beams have the monolayer mode period, monolayer and bilayer mode oscillations for the specular beam are quali-
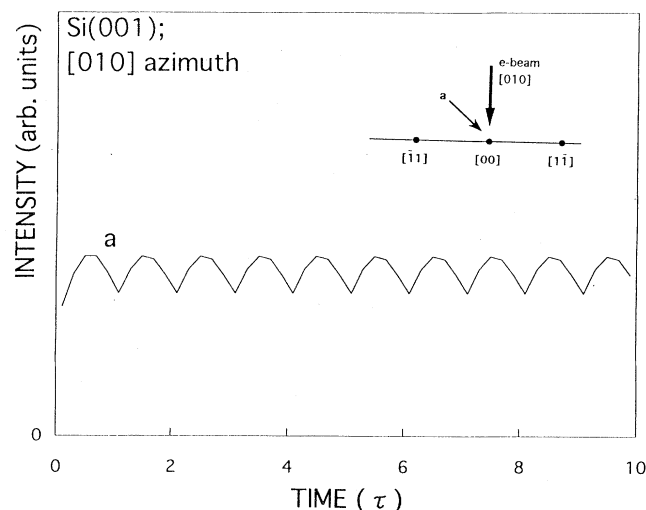
FIG. 6. The result of 3-beam calculation of RHEED intensity oscillations in the [010] azimuth. Inset figures show the reciprocal lattice points of (001)2×1+1×2 taken into the calculation.

tatively reproduced by the three-beam calculations. Then, it is possible to conclude that a Si(001) surface gives rise to monolayer and bilayer mode oscillations for the specular beam at the $[1\bar{1}0]$ and $[010]$ azimuthal directions, respectively, irrespective of the 2×1 and 1×2 surface reconstruction.

Although the multiple-scattering calculations including the 1×2 and 2×1 surface reconstruction beams reproduced the experimental intensity oscillations much better, as Figs. 3 and 4 show, our three-beam calculations suggest that the azimuthal dependence of the RHEED intensity oscillation periods may essentially stem from the periodicity of the diamond structure.

IV. CONCLUSION

We have shown that the multiple-scattering theory combined with the birth-death model can reproduce well the RHEED oscillation modes without steps. The monolayer and bilayer mode oscillations are mainly caused by the interaction among the specular, two side bulk and two surface reconstruction beams on the zeroth Laue zone, and the key to this is the periodicity of these beams against surface normal direction. Of course, a real surface during MBE growth has elongated islands, surface reconstruction, and steps. Further study is necessary to clarify the contribution of these surface structures to the RHEED intensity oscillations.

[1] J. Neave, P. Dobson, B. Joyce, and J. Zhang, Appl. Phys. Lett. **47**, 100 (1985).

[2] J. Harris and B. Joyce, Surf. Sci. **103**, L90 (1981).

[3] T. Sakamoto, H. Funabashi, K. Ohta, T. Nakagawa, N. Kawai, and T. Kojima, J. Appl. Phys. **23**, L657 (1984).

[4] T. Sakamoto, N. Kawai, T. Nakagawa, K. Ohta, and T. Kojima, Appl. Phys. Lett. **47**, 617 (1989).

[5] T. Sakamoto, T. Kawamura, and G. Hashiguchi, Appl. Phys. Lett. **48**, 1612 (1986).

[6] K. Sakamoto, T. Sakamoto, K. Miki, and S. Nagao, J. Electrochem. Soc. **136**, 2705 (1989).

[7] R. Farrow, S. Parkin, P. Dobson, J. H. Neav, and A. Arrott, *Thin Film Growth Techniques for Low-dimensional Structures* (Plenum, New York, 1987).

[8] N. Ohtani, S. Mokler, J. Zhang, and B. Joyce, Appl. Phys. Lett. **61**, 21 (1992).

[9] T. Kawamura, T. Sakamoto, and K. Ohta, Surf. Sci. **171**, L409 (1986).

[10] T. Kawamura, T. Sakamoto, and P. Maksym, Surf. Sci. **181**, L171 (1987).

[11] Z. Mitura, M. Stróżak, and M. Jalchowski, Surf. Sci. Lett. **276**, L15 (1992).

[12] D. J. Chadi, Phys. Rev. Lett. **43**, 43 (1979).

[13] M. T. Yin and M. L. Cohen, Phys. Rev. B **24**, 2303 (1981).

[14] I. P. Batra, Phys. Rev. B **41**, 5048 (1990).

[15] P. Cohen, G. Petrich, P. Pukite, J. Whaley, and A. Arrott, Surf. Sci. **216**, 222 (1989).

[16] J. Weeks and G. Gilmer, Adv. Chem. Phys. **40**, 157 (1979).

[17] A. Ichimiya, Jpn. J. Appl. Phys. **22**, 176 (1983).

[18] A. Ichimiya, Surf. Sci. **235**, 75 (1990).

[19] P. A. Maksym and J. L. Beeby, Surf. Sci. **110**, 423 (1981).

[20] T. Kawamura, A. Ichimiya, and P. Maksym, Jpn. J. Appl. Phys. **27**, 1098 (1988).

[21] Z. Mitura and P. A. Maksym, Phys. Rev. Lett. **70**, 2904 (1993).